



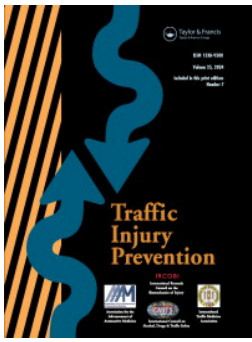
Quantifying rider posture variability in powered two- and three-wheelers for safety assessment

Downloaded from: <https://research.chalmers.se>, 2024-10-26 12:15 UTC

Citation for the original published paper (version of record):

Lundin, L., Oikonomou, M., Lioras, A. et al (2024). Quantifying rider posture variability in powered two- and three-wheelers for safety assessment. *Traffic Injury Prevention*, 25(7): 956-967.
<http://dx.doi.org/10.1080/15389588.2024.2351607>

N.B. When citing this work, cite the original published paper.



Quantifying rider posture variability in powered two- and three-wheelers for safety assessment

Linus Lundin, Maria Oikonomou, Athanasios Lioras, Athanassios Mihailidis, Bengt Pipkorn, Lambros Rorris, Mats Y. Svensson & Johan Iraeus

To cite this article: Linus Lundin, Maria Oikonomou, Athanasios Lioras, Athanassios Mihailidis, Bengt Pipkorn, Lambros Rorris, Mats Y. Svensson & Johan Iraeus (2024) Quantifying rider posture variability in powered two- and three-wheelers for safety assessment, Traffic Injury Prevention, 25:7, 956-967, DOI: [10.1080/15389588.2024.2351607](https://doi.org/10.1080/15389588.2024.2351607)

To link to this article: <https://doi.org/10.1080/15389588.2024.2351607>



© 2024 The Author(s). Published with license by Taylor & Francis Group, LLC.



[View supplementary material](#)



Published online: 20 Jun 2024.



[Submit your article to this journal](#)



Article views: 541







[View related articles](#)



[View Crossmark data](#)

Quantifying rider posture variability in powered two- and three-wheelers for safety assessment

Linus Lundin^a , Maria Oikonomou^b, Athanasios Lioras^c, Athanassios Mihailidis^b, Bengt Pipkorn^{a,d} , Lambros Rorris^e, Mats Y. Svensson^a  and Johan Iraeus^a 

^aDepartment of Mechanics and Maritime Sciences, Chalmers University of Technology, Gothenburg, Sweden; ^bSchool of Mechanical Engineering, Aristotle University of Thessaloniki, Thessaloniki, Greece; ^cCrash and Safety Department, BETA CAE Systems SA, Thessaloniki, Greece; ^dAutoliv Research, Vårgårda, Sweden; ^eCrash and Safety Department, BETA CAE Systems International AG, Luzern, Switzerland

ABSTRACT

Objective: Injury outcomes for powered two- and three-wheeler (PTW) riders are influenced by the rider posture. To enable analysis of PTW rider accidents and development of protection systems, detailed whole-body posture data is needed. Therefore, the aim of this study is to fill this gap by providing collections of average male whole-body postures, including subpopulation variability, for different PTW types. This will enable future studies to explore the influence of PTW rider posture variation and to support safety system development.

Methods: 3D photometric measurements of 51 anatomical landmarks were recorded on 20 (50th percentile male) volunteers in their preferred riding postures across three PTW types (naked, scooter, and touring). Following an outlier removal process, a principal component analysis (PCA) was performed to calculate average postures and principal components (PCs), to describe the observed posture variation, for each PTW. The visualization of the PCs was facilitated through kinematic linkage representations, connecting anatomical landmarks and estimated joint centers to form segments and characteristic joint angles.

Results: The first seven PCs explained 80% of the variance in posture for each of the three PTWs. Across PTWs, these PCs frequently described combinations of postural features including variation in fore-aft seat positions, pelvic tilt, spinal curvature, head position, and extremity flexion-extension. Analysis revealed distinct differences in average postures across the three PTWs, on average, $10 \pm 9^\circ$ for the characteristic joint angles within a min-to-max range between the three PTWs. However, for all three PTWs, the variability between volunteers in characteristic joint angles on the same PTW were on average more than twice as large within a ± 2 SD range ($26 \pm 11^\circ$).

Conclusions: The results suggest that PTW rider posture variation must be addressed by involving simultaneous adjustments of multiple body parts, as described by each of the first seven PCs, as a direct consequence of the human body interconnectedness. Furthermore, the study's findings challenge conventional assumptions that the relative distance between PTWs' handlebar, seat, and foot support predominantly influences rider postures. Instead, the research demonstrates that individual variability has a substantial influence on rider posture and should be considered in PTW safety development.

ARTICLE HISTORY

Received 8 February 2024

Accepted 1 May 2024

KEYWORDS



Motorcycle; powered two- and three-wheeler; vulnerable road user; posture variability; principal component analysis


Introduction

Powered two- and three-wheelers (PTWs) are a widely used transportation mode. They are especially popular in countries like Indonesia, Vietnam, and India, constituting over 70% of the total vehicle fleet (ITF, 2015; Huu and Ngoc 2021). Regardless of geographical location, PTW riders are recognized as vulnerable road users, with their share of road traffic fatalities ranging from 10% in Europe, 14% in the United States, to more than 40% in Southeast Asia (ITF, 2015; NCSA, 2023). Over the period 2010–2019; drawing on data from 34 countries

worldwide, the average number of PTW fatalities increased by 7% (ITF, 2022), emphasizing the need to enhance PTW safety.

Passive safety systems demonstrate promise for enhancing PTW rider safety (Capitani et al. 2010; Thollon et al. 2010; Ariffin et al. 2016; Maier et al. 2022; Maier and Fehr 2024). However, to maximize their effectiveness, the variability of PTW crashes needs to be addressed (ISO 13232-6:2005 2005; Rogers and Zellner 2001; Barbani et al. 2014). This includes variability in rider postures, which have been reported to influence the injury outcome for the two most frequently seriously injured (AIS2+) body regions – head

CONTACT Linus Lundin  linus.lundin@chalmers.se  Department of Mechanics and Maritime Sciences, Chalmers University of Technology, Hörsalsvägen 7A, SE-412 58 Göteborg, Sweden.

 Supplemental data for this article can be accessed online at <https://doi.org/10.1080/15389588.2024.2351607>.

Associate Editor Jason Forman oversaw the review of this article.

© 2024 The Author(s). Published with license by Taylor & Francis Group, LLC.

This is an Open Access article distributed under the terms of the Creative Commons Attribution License (<http://creativecommons.org/licenses/by/4.0/>), which permits unrestricted use, distribution, and reproduction in any medium, provided the original work is properly cited. The terms on which this article has been published allow the posting of the Accepted Manuscript in a repository by the author(s) or with their consent.

and chest (Langwieder 1977; Schaper and Grandel 1985; Sporner et al. 1990; Wisch et al. 2019; Gidion et al. 2021).

Despite the influence of posture on injury outcome, PTW rider surrogates, such as physical and virtual anthropometric test devices (ATDs) or finite element human body models (HBMs), are for each study, typically positioned in only one nominal rider posture (ISO 13232-6:2005 2005; Capitani et al. 2010; Prochowski and Pusty 2013; Ariffin et al. 2016; Bonkowski et al. 2020; Maier et al. 2021; 2022). This practice reflects the belief that accommodating PTW operation requirements precedes individual preferences in posture adaptation (Claffin 2002), assuming that PTW rider postures are almost exclusively determined by the spatial relationship between the handlebar, seat, and foot support i.e., the “ergonomic triangle” (Sabbah and Bubb 2008; Arunachalam et al. 2019).

Incorporating posture variability into PTW safety research is challenging due to a lack of detailed posture data required for precise positioning of human surrogates, such as HBMs. Existing studies on PTW rider posture have focused on ergonomics in PTW design, employing a simplified kinematic linkage model with body landmarks defining segments and joint angles (Arunachalam et al. 2019). These ergonomic posture models are not suitable for positioning HBMs due to several limitations. These limitations include the absence of joint angles in all three anatomical planes (Chou and Hsiao 2005; Arunachalam et al. 2019, 2021), and the misrepresentation of joint centers through the direct connection of skin-based markers (Barone and Curcio 2004). Additionally, if spinal loading is to be investigated for PTW riders using similar demands as the approach previously applied to car occupants in various postures during frontal crashes (Izumiyama et al. 2022), accurate spinal column curvature representation is necessary. To achieve precision, representing spinal column curvatures should extend beyond the common practice of using only one or two angles, as observed in PTW posture studies by Barberi et al. (2023), Barone and Curcio (2004), Smith et al. (2006), and Van Auken et al. (2005).

However, another obstacle to integrating posture variation into PTW safety assessment lies in the lack of documented variability. Current studies typically only present average postures using average joint angles and occasionally include angle-specific standard deviation or range values, for every joint in isolation (Barone and Curcio 2004; Chou and Hsiao 2005; Van Auken et al. 2005; Smith et al. 2006; Sabbah and Bubb 2008). This means that this limited data representation fall short in considering variation at a holistic, whole-body level. Access to whole-body posture variation data would allow developers of safety systems to evaluate the safety benefit for both average and alternative rider postures, incorporating a known degree of posture diversity.

Principal component analysis (PCA) has been used as a dimensionality reduction method for investigating posture variation in extensive landmark-based datasets in sport applications (Federolf et al. 2014) and for predicting body sizes and shapes in ergonomics applications (Reed et al. 2014). Yet, it remains unexplored in PTW posture applications. Briefly, PCA creates new uncorrelated variables

referred to as principal components (PCs) from linear combinations of the variables found in a dataset. The PCs are sorted based on how much variance they explain. Typically, the first few PCs cumulative explains a majority of the total variance (Jolliffe and Cadima 2016). Collectively, these PCs establish a new basis for interpreting and quantifying the posture variability in datasets that might otherwise be challenging to comprehend.

The paper’s objective is to provide collections of rider posture variation through kinematic linkage representations utilizing joint center-based angles in all three anatomical planes. This data will fill an important gap in the existing PTW safety research and allow future studies to explore the influence of PTW rider posture variation, ultimately contributing to the development of safety systems aimed at reducing the risk of injury in PTW accidents.

Methods

The methods section is divided into five subsections. The first subsection describes the experimental setup used to obtain the posture measurements. The second subsection outlines how the PCA was implemented. The third to fifth subsections define the procedure used to identify and remove inconsistent marker repetitions, how the skinfold thicknesses at different marker locations were accounted for, and the methods used for the joint and the characteristic angle calculations.

Experimental data collection

Twenty volunteers were included in the study. All volunteers provided written informed consent, and the research received ethical approval from the “Research Ethics Committee of the Universitat Politècnica De València” under protocol number P04_18-10-2022. The volunteers were chosen based on height and weight criteria, aligning with average male specifications defined in Schneider et al. (1983). The target values were 175 cm for height and 77 kg for weight. The selected volunteers’ characteristics, ranging from 171.5 to 178.6 cm in height and 71.1 to 82.1 kg in weight, were measured using a stadiometer with an accuracy of 1 mm and an electronic bascule with an accuracy of 0.1 kg. No volunteers reported pre-measurement issues related to the spinal column or balance. More information about volunteers’ characteristics can be found in Table A1 (Appendix A, supplementary material).

Each volunteer was measured in five different postures, which included standing, sitting on a stool, and riding three types of PTWs: naked, scooter, and touring. These PTWs represent different bike segments, with different relative distances between the handlebar, seat, and foot support, see Figure 1. Photos of the standing and seated postures can be observed in Figure A1 (Appendix A, supplementary material). The measurements were recorded in three sessions. During the first, the standing posture and the posture of the volunteer riding the naked PTW were recorded. In the second session, the posture of the volunteer sitting on a stool with a straight back and riding the scooter PTW were measured.



Figure 1. Measuring process of a volunteer positioned on the three PTWs: naked (A), scooter (B), and touring (C).

In the final session, the posture of the volunteer riding the touring PTW was captured.

The measurement procedure was performed in a photogrammetric laboratory equipped with 12 cameras and Kinescan/IBV recording software (IBV, 2014). The software can detect reflective markers at 30Hz with a spatial accuracy of 1mm. In addition, the skinfold thickness was measured at each marker location using a caliper with an accuracy of 0.2mm.

In detail, 51 flat reflective markers were positioned on the skin adjacent to anatomical landmarks identified through palpation. The palpation was individually conducted by one of the two experienced physiotherapists involved in the project. These anatomical landmarks were considered characteristic points of the human body, and information about their location was used to document the human posture. This set of markers included 5 markers on the volunteer's head, 14 on the arms, 4 on the scapulae, 2 on the clavicles, 4 on the hips, 14 on the legs, and 8 on the spine. Figure 2 illustrates the position of the reflective markers on the volunteers' skin. More information about the exact location of each marker can be found in Table A2 (Appendix A, supplementary material).

Six additional spherical markers were placed on each of the PTWs to provide information about the PTWs' 3D position and the volunteers relative position to the PTW. These points correspond to the PTWs' rear and forward wheels and most fore and aft points, displayed in Figure A2 (Appendix A, supplementary material).

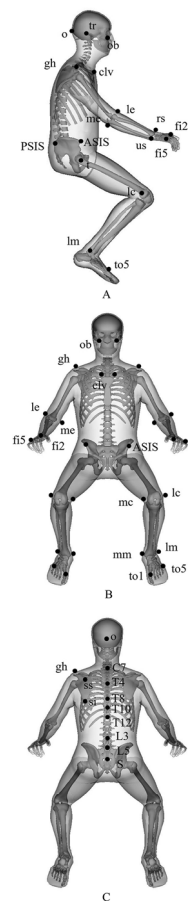


Figure 2. Reflective markers' position on the human in a PTW rider posture. Identical markers are placed on left and right extremities. Side view (A), front view (B), rear view (C).

The measuring procedure included the following steps: First, if a PTW was involved, spherical markers were placed on the PTW. Then, the volunteer positioned himself with his gaze focused on a rearview-sized mirror, positioned in front of the volunteer at the same height as his eyes to mimic riding straight ahead. Subsequently, three skinfold measurements were taken for each anatomical landmark. Finally, reflective markers were placed on the volunteer's anatomical landmarks, and three repeated measurements of the volunteer in the desired posture were captured. The repeated measurements were conducted consecutively, and each one was a 3-s-long video to ensure that none of the marker measurements were affected by small motions.

In cases involving PTWs, some reflective markers were hidden by the PTW, making it not possible for these to be identified by the minimum required number of cameras. Thus, to extract their position, a specific calibrated tool was employed. This tool features a metal rod with a pointed tip at one end and a Y-shaped attachment at the other. The Y-shaped attachment is equipped with three spherical markers, placed at each end of its branches. During PTW postures, the tool's tip was placed on each hidden marker before conducting skinfold measurements, and three 5-s videos were recorded. The position of the hidden marker was then calculated based on the position of the three spherical markers on the tool.

Principal component analysis

PCA with mean centering was employed for each PTW to linearly transform the dataset comprising 3D measurements from all volunteers. First, the volunteer measurements were organized as a n -by- p matrix \mathbf{X} , where n represents the number of observations (volunteers, 20), and p denotes the number of variables (3 dimensions \times 51 markers = 153 variables). Each of the variables p corresponds to the average X-, Y-, and Z-coordinates of the available number of repetitions of each skin-based marker. This allowed maximum two of the available three repetitions of each marker to potentially be considered inconsistent and removed without the need for imputation. Next, the PCA was conducted using the MATLAB Statistics and Machine Learning Toolbox (R2023b, The MathWorks Inc., Natick, MA, US). The function *pca* was applied, taking the data matrix \mathbf{X} as input for the analysis.

The output included the principal loadings, represented by a p -by- $(n-1)$ matrix $\mathbf{L} = (l_{ij})_{1 \leq i \leq p, 1 \leq j \leq (n-1)}$. Rows of \mathbf{L} describe variables, and columns describe PCs, ordered in descending order of the explained variance. PC scores, described by a n -by- $(n-1)$ matrix were also obtained, describing the representations of \mathbf{X} in the new basis formed by the PCs. The PC scores translate to how much each volunteer aligns with each PC. Additionally, a 1-by- $(n-1)$ vector $\boldsymbol{\mu}$, representing the estimated mean of each variable in \mathbf{X} (average posture) were computed, as well as the explained variance for each PC.

The standard deviation (σ_i) for each PC score was calculated, enabling the calculation of marker coordinates that correspond to postures aligned with ± 2 SDs or roughly 95% of the observed variability for each PC. The process for determining these ± 2 SD postures is outlined by Equation (1).

$$\text{sample posture } \mathbf{k} = \boldsymbol{\mu} + k\sigma_i \mathbf{l}_i, \quad k \in \{-2, 2\}, 1 \leq i \leq (n-1) \quad (1)$$

Outlier removal methodology

To ascertain the reliability of the photogrammetric measurements, a comprehensive quality check was conducted on the marker measurements of all participants across the five postures. The data from each participant was examined separately, and the distances between the successive markers were linked to form segment lengths. Given the expected constancy of each volunteer's segment lengths across all postures, it was assumed that the distance between successive markers should remain constant. However, slight variations in the calculated distances within a specified tolerance were expected due to the repositioning of markers between the five postures and the associated skin-to-bone movement.

For each participant, 67 segment lengths were defined: 27 on the upper extremities, 18 on the lower extremities, and 22 on the head and pelvis region. As elaborated below, a separate methodology was employed to analyze the spine region. For each of the 67 defined segment lengths, 15 distances were determined for each volunteer (3 repetitions \times 5 postures = 15 distances). The mean and standard deviation of each segment length were computed from the 15 distances. Each of the 15 distances was tested against the

chosen tolerance. If a distance value exceeded the acceptable limits, it was deemed inconsistent. The acceptable limits are expressed as $(\text{mean} - \text{tolerance}) \leq \text{distance value} \leq (\text{mean} + \text{tolerance})$. In case a distance value was outside the tolerance, the two markers' repetition that form the corresponding distance were flagged as potentially inconsistent.

Upon examining distances across all 67 defined segment lengths for a given participant, all inconsistent distances and all potentially inconsistent markers were identified. Then, the number of times that each marker was flagged as potentially inconsistent was calculated. For each identified inconsistent distance, one of the corresponding potentially inconsistent markers' repetition had to be removed. The criterion for marker repetition removal was based on the frequency of being flagged as potentially inconsistent, with a preference for the marker repetition flagged more frequently. Both markers' repetition were removed in cases of equal flagging frequency.

In the spine region, markers were placed on the skin adjacent to the spinous processes of the C7, T4, T8, T10, T12, L3, and L5 vertebrae. The lack of information regarding the locations of all vertebrae would result in the formation of larger segments that span several vertebrae, as illustrated in Figure A3 (Appendix A, supplementary material). However, given the varying spinal curvature in different human postures, the lengths of these formed segments may also vary. Therefore, assuming a constant length for these segments is inaccurate. To address this, a separate approach was adopted to check spine measurements quality. The quality check in this region ensured the correct spatial alignment of markers along the Z-axis, with markers verified to have decreasing Z-value from C7 to L5 vertebra.

A metric named Mean Average Difference (MAD) was derived to quantify how much the PCs, describing the posture variation, changed as an increasing number of marker repetitions were systematically identified as inconsistent and removed from the input data (\mathbf{X}). First, the euclidean distance was calculated between each marker position ($k = 51$) for the baseline data (a) and the data with inconsistent marker repetitions removed (b) corresponding to the +2 SD postures for each PC. Then, as seen in Equation (2), the average value of all the euclidean distances for each of the $(n-1)$ PCs was computed. Finally, the average euclidean distances for the PCs were averaged over all three PTWs to form the total MAD. The total MAD metric describes how much the posture variation explained by the PCs change

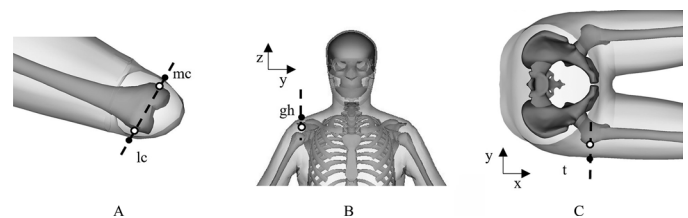


Figure 3. Skinfold thickness removal. In the elbow, wrist, knee, and ankle joints the correction was driven by the assumed linearity (A). In the shoulder region the correction was in the direction of Z-axis (B). In the hip region the correction was in the direction of Y-axis (C).

when removing specific amounts of marker repetitions compared to the original dataset.

$$\text{MAD}^{\text{PCs}} = \frac{\sum_{i=1}^k \|b_i - a_i\|}{k}, k = 51 \quad (2)$$

Increasingly strict tolerance for the outlier removal, corresponding to an increasing number of marker repetitions removed, were tested using the total MAD metric. This was used to determine the least strict tolerance that removed the incorrect measurements while preserving the maximum amount of variance in the dataset. At least one marker repetition for all volunteers, in all postures, was needed to avoid imputation. Starting from a tolerance equal to 3 SD of the 15 distances of each segment length, the tolerance was iteratively reduced until reaching the minimum value of 2 SD.

Skinfold thickness removal

Two methods were used to remove the skinfold thickness across the volunteers' joints to give a more accurate representation of the underlying bone structures. The first method was implemented for joints characterized by two markers positioned at the lateral and medial sides, encompassing the elbow, wrist, knee, and ankle joints. This method assumes that the anatomical landmarks of the bones align linearly with their corresponding skin anatomical landmarks. Consequently, the skinfold thickness, taken at the markers' location on the skin, were removed in the direction aligned with the assumed rotational axis, as depicted in Figure 3A. The initial skin landmarks are depicted with black filled dots, and the corresponding estimated bone landmarks are illustrated with white dots.

The second method was utilized for shoulder and hip joints, where skinfold distribution was considered along a specific axis. For shoulder measurements, as shown in Figure 3B, skinfold distribution was assumed along the Z-axis, while for hip joints, Figure 3C, skinfold distribution was assumed along the Y-axis.

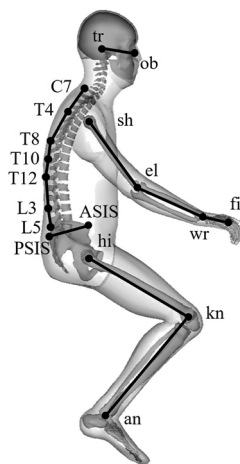


Figure 4. Kinematic linkage representation.

Joints and characteristic angles calculation

Following the PCA, a kinematic linkage model was developed representing the human musculoskeletal system. This model consists of the human joint centers and anatomical landmarks connected by the in-between body segments, similar to Chou and Hsiao (2005) and Reed et al. (1999). However, in cases where the data are collected on volunteers' skin, estimating joint centers requires further calculations. In this study, various methods applied in previous studies were utilized to estimate the volunteers' joint centers following the PCA. The utilized equation for each joint center can be found in Table B1 (Appendix B, supplementary material).

The elbow, wrist, knee, and ankle areas were characterized by two markers positioned at the lateral and medial sides of the joints. Consequently, these joint centers were estimated as the average point of the corresponding lateral and medial markers.

For the shoulder joint, the center was estimated according to Rab et al. (2002) using the "gh" marker, which was placed on the most dorsal point on the acromioclavicular joint shared with the scapula. This method places the joint center at a distance below the "gh" marker (in the Z-direction). The distance equals 17% of the shoulder width (left "gh"-to-right "gh" distance) according to Rab et al.

The hip joint center calculation was based on Weinhandl and O'Connor (2010), using the trochanter "t" marker. The joint center was estimated to be 25% of the trochanter-to-trochanter distance, positioned medially from the "t" marker, in the corresponding trochanter-to-trochanter direction.

A kinematic linkage representation was developed using 30 points (joint centers and anatomical landmarks) on the

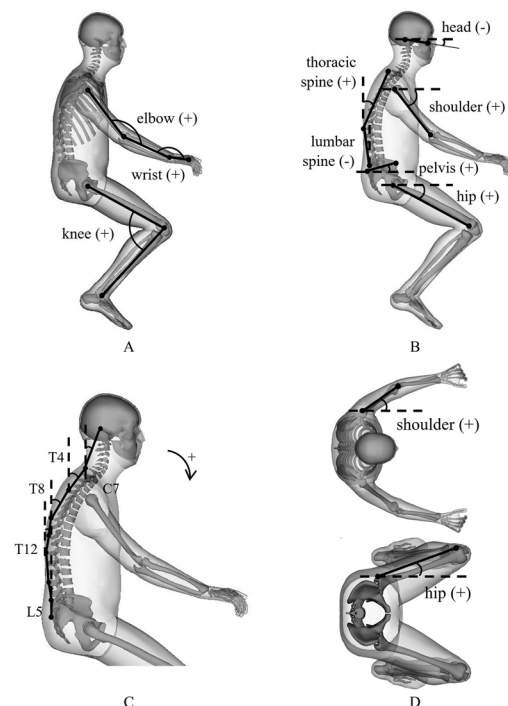


Figure 5. Characteristic angles for the kinematic linkage model: segment to segment angles (A), mid-sagittal plane angles (B), mid-sagittal plane spine angles (C), and horizontal plane angles (D). The parentheses indicate the angles' polarity, except in (C), where the polarity is indicated by the arrow.

human body, as seen in Figure 4. The representation included four points on each lower extremity representing the trochanter, hip, knee, and ankle joints, four points on each upper extremity representing the shoulder, elbow, wrist joints, and the finger, two on the head to form the Frankfort plane, four on the pelvis representing PSIS and ASIS points, and another eight on the spine representing the spinous processes of C7, T4, T8, T10, T12, L3, and L5 vertebrae.

Subsequently, characteristic angles between the adjacent segments, such as elbow, wrist, and knee angles, were calculated using Equation (3), where \mathbf{a} and \mathbf{b} represents the vectors formed between the ends of the two segments.

$$\theta = \cos^{-1} \left(\frac{\mathbf{a} \cdot \mathbf{b}}{\|\mathbf{a}\| \|\mathbf{b}\|} \right) \quad (3)$$

Moreover, characteristic angles between specific segments and anatomical planes were calculated. The angles formed between a segment and the mid-sagittal plane, such as head, vertebrae, pelvis, shoulder, and hip were calculated by Equation (4). The angles formed between a segment and the horizontal plane, such as hip, were calculated by Equation (5). Finally, the angles formed between a segment and the frontal plane, such shoulder, were calculated by Equation (6).

$$\theta_{xz} = \tan^{-1} \left(\frac{\Delta z}{\Delta x} \right) \quad (4)$$

$$\theta_{xy} = \tan^{-1} \left(\frac{\Delta y}{\Delta x} \right) \quad (5)$$

$$\theta_{yz} = \tan^{-1} \left(\frac{\Delta z}{\Delta y} \right) \quad (6)$$

These characteristic angles including their polarity are illustrated in Figure 5. Further details regarding the calculation of characteristic angles can be found in Table B2 (Appendix B, supplementary material).

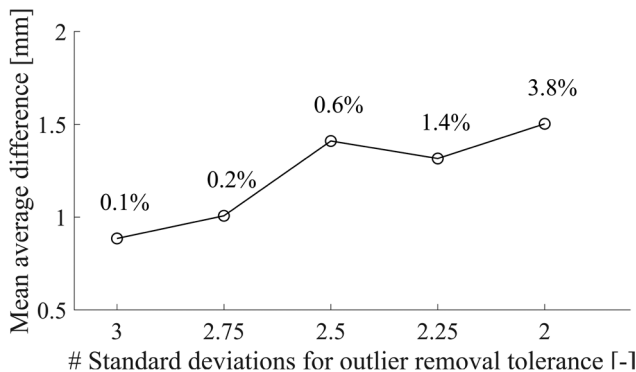


Figure 6. Total MAD, as detailed in the methods section, across various datasets corresponding to increasingly strict inconsistent marker repetition removal thresholds. The accompanying percentage of eliminated marker repetitions is presented above each data point.

Results

The total MAD was calculated, as detailed in the methods, for six different tolerances ranging from less to more strict (3 SD to 2 SD of the 15 distances of each segment length). Figure 6 illustrates the impact of varying tolerances on the total MAD values. The least strict tolerance of 3 SD, with minimal marker repetition removal, resulted in a total MAD closest to zero. This corresponds to a posture variation most similar to that described by the PCs in the original dataset. By making the threshold stricter (from 3 SD to 2.5 SD), the MAD increased by 0.53mm. This signifies that the removed repetitions influence the postural features described by the PCs. However, between 2.5 SD and 2 SD the MAD remains within an absolute difference of 0.19mm. This means that the additional removal of marker repetitions for a threshold stricter than 2.5 SD had minimal effect on the PCs. Subsequently, the analysis

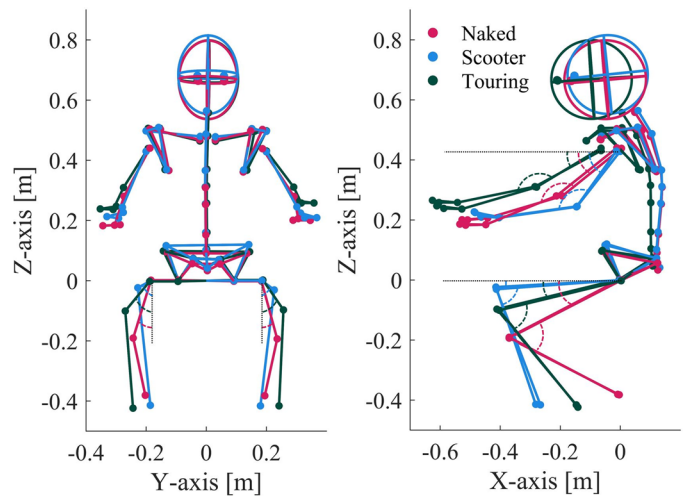


Figure 7. Kinematic linkage representation of the average postures for the three PTW types: naked (red), scooter (blue), and touring (green), rear view (left) and side view (right) with the mid-hip position aligned at the origin (X, Y, Z=0, 0, 0).

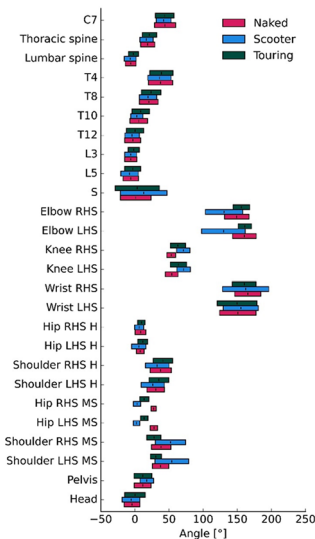


Figure 8. Bars represent the ± 2 SD range indicating intra-variability, while vertical lines denote average angles for each PTW (naked, scooter, and touring). MS=mid-sagittal plane, H=horizontal plane.

employed a dataset where 0.6% of all marker repetitions were considered inconsistent and removed using a threshold of 2.5 SD of the 15 distances of each segment length.

In Figure 7, the average postures of the 20 volunteers across three types of PTWs are presented using the kinematic linkage model, with the mid-hip position aligned at the origin ($X, Y, Z=0, 0, 0$). Figure 7 is complemented by Figure 8, illustrating both the inter-variability in angles for the three average postures and the intra-variability between volunteers on the same PTW, represented by the ± 2 SD range per angle.

The largest differences among the three average postures (inter-variability) are observed in the side view (Figure 7), particularly in the hip angle (ranging from 5° for scooter to 27° for naked, relative to the X-axis), knee angle (ranging from 54° for scooter to 74° for naked), shoulder angle (ranging from 30° for touring to 54° for scooter, relative to the X-axis), and elbow angle (ranging from 131° for scooter to 160° for touring) (Figure 8).

In contrast, there is a close resemblance in thoracic spine curvature (within 5°) among the three average postures (Figure 7 and 8). Although, the average touring posture has an increased forward lean indicated by marginally larger spine angles (Figure 8). This increased forward lean may be attributed to a longer seat-to-handlebar distance, suggested by the higher and more forward hand placement compared to the other two postures.

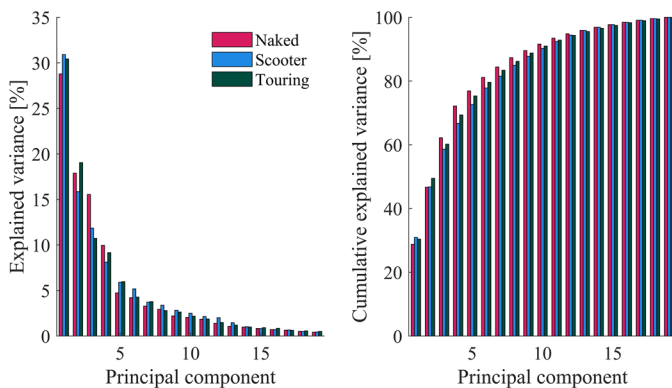


Figure 9. Explained variance for each principal component (left), and the cumulative explained variance (right) for the three PTW types: naked (red), scooter (blue), and touring (green).

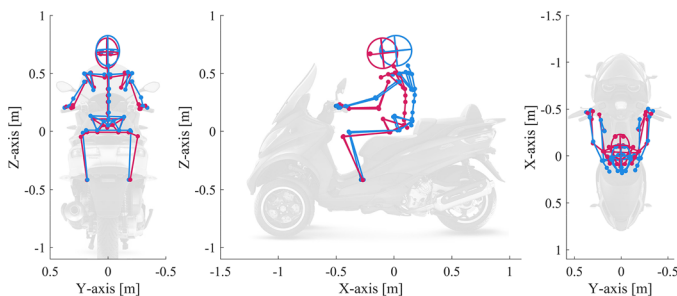


Figure 10. Kinematic linkage model illustrates ± 2 SD postural features along scooter PC 1, with PTW background image for illustration purposes. Note: stick-man vs. PTW comparisons are unreliable due to non-comparable suspension travel and possible distortion effects. Background photo ©piaggio.

The PCA resulted in 19 (number of volunteers – 1) non-zero PCs, collectively describing the total posture variation of the dataset. Figure 9 displays the variance explained by each PC, including the cumulative counterpart. The difference in explained variance, across the same PC for the different PTWs, did not exceed five percentage units. Consequently, the first seven PCs cumulatively explained at least 80% of the posture variance for all three PTWs. However, beyond PC 4, the decrease in explained variance appeared to stabilize, indicating marginal differences among subsequent PCs. The average postures for the three PTWs, the PC loadings, and standard deviations of the PC scores for the first seven PCs can be seen in Appendix E, supplementary material.

Using the kinematic linkage model described in the methods, the differences from the average posture for each PC and PTW combination was illustrated with two postures corresponding to ± 2 SD (roughly 95% of the variability) from the mean PC scores. Figures 10–12 illustrate the ± 2 SD variability for scooter PC 1–3. Accordingly, these first three PCs show the most distinctive variations across all three PTWs. The first PC (Figure 10) accounted for 31% of the variance for the scooter. It described features relative to the average posture corresponding to fore-aft sitting position (± 38 mm in X, measured at mid hip), hip abduction-adduction ($\pm 4^\circ$), flexion-extension of shoulder ($\pm 17^\circ$), and elbow ($\pm 22^\circ$) joints.

Scooter PC 2 (Figure 11) explained 16% of the variance, involving anterior-posterior pelvic tilt ($\pm 2^\circ$), changes in upper body sitting height, and associated adjustments in head position and pitching. Because of the change in sitting

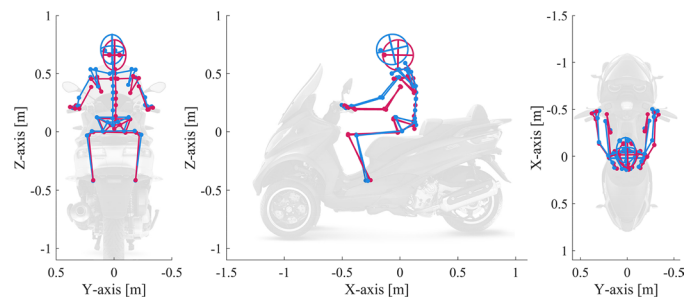


Figure 11. Kinematic linkage model illustrates ± 2 SD postural features along scooter PC 2, with PTW background image for illustration purposes. Note: stick-man vs. PTW comparisons are unreliable due to non-comparable suspension travel and possible distortion effects. Background photo ©piaggio.

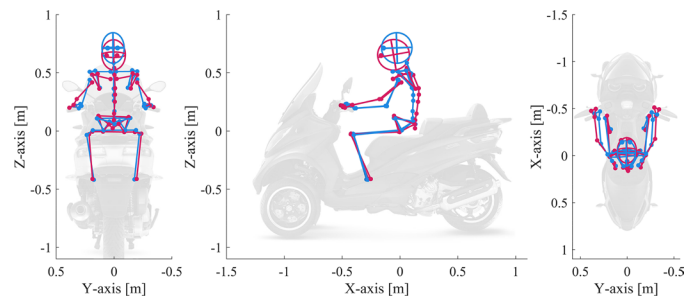


Figure 12. Kinematic linkage model illustrates ± 2 SD postural features along scooter PC 3, with PTW background image for illustration purposes. Note: stick-man vs. PTW comparisons are unreliable due to non-comparable suspension travel and possible distortion effects. Background photo ©piaggio.

Table 1. Explained variance and characterized variation in postural features observed for the first three PCs for the naked and touring PTWs.

| PTW | PC # | Explained variance [%] | Characterized variation |
|---------|------|------------------------|---|
| Naked | 1 | 29 | <ul style="list-style-type: none"> • LHS lean • Anterior-posterior pelvic tilt • Higher-lower head position |
| | 2 | 18 | <ul style="list-style-type: none"> • LHS-RHS lean • Curved-straight spine • Flexion-extension elbow • Flexion-extension wrist |
| | 3 | 16 | <ul style="list-style-type: none"> • Anterior-posterior pelvic tilt • Abduction-adduction hip |
| Touring | 1 | 30 | <ul style="list-style-type: none"> • Anterior-posterior pelvic tilt • Curved-straight spine |
| | 2 | 19 | <ul style="list-style-type: none"> • Fore-aft sitting position • LHS-RHS lean • Flexion-extension knee |
| | 3 | 11 | <ul style="list-style-type: none"> • Anterior-posterior pelvic tilt • Flexion-extension wrist |

height and pelvic rotation, flexion-extension of the elbow ($\pm 9^\circ$), and knee ($\pm 8^\circ$) occurred to accommodate for the rider-machine interaction points (handlebar and foot support).

Overall, scooter PC 3 (Figure 12) demonstrated similar features as scooter PC 2. Although, no change in sitting height was observed, and only half the magnitude for the flexion-extension of the knee joint ($\pm 4^\circ$) was recorded. Instead, there were larger differences in spine curvature and abduction-adduction of the shoulders ($\pm 12^\circ$) because of altered hand position. The changed hand position involved a wider-narrower placement and fore-aft movement. The latter was a result of volunteers' choosing to rest four fingers on the brake levers with the thumb placed on top of the handlebars, as opposed to the more frequently seen closed grip with the thumb wrapped around the handlebar.

Table 1 (together with figures in table C1 Appendix C, supplementary material) complements the scooter results by showcasing the characterized features observed in the first three PCs for the naked and touring PTWs. Table 1 reveals that, for the most part, the features identified for the first three PCs for the scooter aligns with that observed for the naked and touring PTWs, although with some exceptions. One such exception was the fore-aft sitting position, a feature described by PC 1 for the scooter. Fore-aft sitting position was included in PC 2 for the touring PTW, but did not appear in the first three PCs for the naked PTW. This feature also exemplifies that the order of PCs and the explained variance attributed to each feature differed between the three PTWs.

For the complete visualization and description of the first seven PCs, for which postural feature could be distinguished, the reader is referred to Appendix C, supplementary material, with the corresponding changes in characteristic angles available in Appendix D, supplementary material.

Discussions

In this study, 3D photometric measurements of 51 anatomical landmarks were captured from 20 male volunteers (50th percentile height and weight) in their preferred riding posture on three different PTW types – naked, scooter, and

touring. Subsequently, a PCA was conducted to extract average postures in combination with posture variation for each PTW type.

Comparison of the average postures across the three PTWs revealed the greatest differences in the sagittal plane, and in particular for the flexion-extension of the hip, knee, shoulder, and elbow joints. The first seven principal components (PCs) cumulatively explained about 80% of the posture variance for each of the three PTWs (Figure 9). Moreover, it was only possible to visually distinguish changes in postural features between the ± 2 SD postures for approximately the first seven PCs across all three PTWs. Subsequent PCs represented variance below 4%, with insufficient differences to be visually characterized – effectively considered as noise.

The first seven PCs were frequently associated with (i) fore-aft seat positions, (ii) anterior-posterior pelvic tilt in conjunction with curved-straight spine and changed head position, (iii) flexion-extension of the upper and lower extremities, and (iv) abduction-adduction of the hip (Figure 10–12 and Appendix C, supplementary material). These postural features were found to be consistent in explaining the majority of the observed variance across all three PTW types, although with differences in magnitudes. Nevertheless, the findings suggests that variation in these postural features are the most important to account for in future PTW safety development, independent of PTW type.

The multitude of postural features associated with different body parts in the first few PCs, makes it challenging to isolate the impact of individual features like e.g., fore-aft sitting position. Attempts to create more sparse principal loadings through Sparse PCA (Zou et al. 2006) and Varimax-rotated PCA (MATLAB Statistics and Machine Learning Toolbox R2023b, The MathWorks Inc., Natick, MA, US) were unsuccessful, likely due to the inherently high multicollinearity in the dataset stemming from the interconnectedness of the human body. Thus, despite the initial appeal of quantifying the effect of “one body part variation at the time” for safety assessment, the results emphasize that most postural changes are interconnected, requiring simultaneous adjustments in multiple features to accommodate for the PTW operational

constraints. For instance, a change in fore-aft sitting position, given the same upper body forward lean, necessitates corresponding modifications in elbow flexion-extension to maintain contact with the handlebars.

To mitigate undesired variations in segment lengths resulting from the PCA, the influence from anthropometric differences were minimized by restricting the volunteers to 50th percentile males from one geographical region. Still, differences in sitting height and pelvis shape and size were observed. However, by only measuring 50th percentile men, posture variations caused by differences in anthropometry, sex, and ethnicity were effectively neglected from the analysis. Ensuring alignment between participants' anthropometry, particularly in height, and that of HBMs, is crucial for HBM positioning in PTW rider postures. Large deviations in height between the participant posture and HBM will necessitate adjustments in the target posture to accommodate the PTW operation requirements.

This study represents an initial step aimed at positioning current standard HBMs as PTW riders. Future studies should broaden their scope to include a wider variety of PTWs and a more diverse rider population, utilizing morphed HBMs to accurately represent these rider profiles. For riders, differences in anthropometry can lead to noticeable variations in average postures (Arunachalam et al. 2019). For example, women or smaller males, owing to their lower height, may adopt postures characterized by a more forward position on the seat, extended elbows, and larger knee angles. This posture choice may be accompanied by a more extended spine to improve visibility over the PTW. Conversely, taller rider could prefer a more rearward position on the seat, while still having the option of flexed elbows and knee angles, with a potentially more relaxed spine posture.

The results in terms of average postures align with existing research (Sabbah and Bubb 2008; Arunachalam et al. 2019) in that varying "ergonomic triangles" among PTW types result in varying average rider postures, at least for the lower extremities. Across the three PTWs, substantial variations in fore-aft feet position relative to the seat resulted in knee and mid-sagittal hip joint angles varying about 20°. Despite this difference, both the naked and scooter average postures exhibited similar spinal column shapes. In contrast, the average touring posture displayed more pronounced anterior pelvic tilt and forward lean. This difference in spinal curvature appears to be attributed to a more forward and elevated handlebar position seen for the touring PTW. In contrast, the average touring posture maintains a foot position intermediate between the naked and scooter. The findings suggest that, for the PTW types under investigation, disparities in handlebar relative seat position influences upper body posture, while differences in the relative positions between the foot support and the seat influences knee and mid-sagittal hip joint angles. However, measurements on additional PTWs are needed to confirm the reliability of this finding.

The average postures across the three PTWs exhibited distinct inter-variability, on average, $10 \pm 9^\circ$ across all joints within a min-to-max range. However, an even greater variability was observed when examining the intra-variability

among volunteers positioned on the same PTW, on average exceeding $26 \pm 11^\circ$ across all joints within a ± 2 SD range. The greater intra-variability was consistently observed for nearly all joint angles (19 out of 26) across all PTWs. The exceptions, where the inter-variability joint angle ranges were larger or within five degrees of the intra-variability ranges, were found to correspond to the lower (hip mid-sagittal and knee) and upper extremity (shoulder mid-sagittal and elbow) angles (see Figure 8). This suggests that, for the studied PTW types, the sagittal position of the upper and lower extremities of the rider postures are largely influenced by the rider-machine interaction constraints. In contrast, the wrist, pelvic, head, and spine angles, are instead found to be a consequence of rider preference for the investigated PTWs. Consequently, opposite to the assumption that PTW operation requirements precedes individual preferences in posture adaptation, these results indicate that rider posture is, at least for the studied PTWs, not exclusively determined by the spatial relationship between the handlebar, seat, and foot support.

The coordinates of the markers placed on the skin adjacent to the spinous processes were not translated to the corresponding vertebral centroid or intervertebral disk. This decision stems from a lack of a well-established method for such a transformation. While literature suggests potential approaches like utilizing average vectors (Snyder et al. 1972) or mapping based on an average difference curve derived from paired skin-based markers and radiographs (Bryant et al. 1989), no method has been validated for PTW postures. Additionally, for applications such as positioning the spine of a HBM, it is likely that both a transformation and a polynomial fit to the markers would be necessary. This dual approach is deemed more effective in accommodating variations in spatial positioning of vertebrae between the HBMs and the dataset under consideration.

By employing a skin-to-vertebral centroid method, the PCs presented in this study offer a practical means of positioning and varying the posture of human surrogates such as HBMs on PTWs. This can be achieved either by directly utilizing the comprehensive joint angles across all three anatomical planes (see Appendix D, supplementary material) or by employing skin-based marker coordinates (see Appendix E, supplementary material), which are then translated to the joint centers as outlined in the methods section. This data will allow developers of protective devices to account for the influence of PTW rider posture variation, shown to affect injury outcome (Langwieder 1977; Schaper and Grandel 1985; Sporer et al. 1990). For instance, to enclose 59% of the posture variation specific to a step-through scooter, six simulations of a crash scenario, aligned with the ± 2 SD postures of the first three PCs, would be required. It is plausible that the number of postures required to account for posture variation could be reduced. However, this would require future studies to investigate if all the presented posture variations have similar influence on the injury outcome or interaction with different protective systems.

It's important to acknowledge that a usual posture while riding may not accurately represent the pre-impact

position of riders in all types of accidents. Nonetheless, there is evidence supporting the use of a usual rider posture for positioning human surrogates in various crash simulations. Langwieder (1977) observed that in over 90% of PTW accidents studied (N=1016), riders maintained their normal riding posture due to the sudden nature of accidents, leaving no time for reaction. Han et al. (2017) found that at least 25% of bicycle and PTW riders in their sample (N=200) did not engage in emergency avoidance maneuvers (22% uncategorized), with a similar trend noted in the Motorcycle Accidents In-Depth Study (MAIDS) (ACEM, 2009), where about one-third of accidents (N=1346) involved no attempt at collision avoidance. Braking was the sole avoidance action in half of the accidents in the MAIDS (ACEM, 2009). Thus, combining active HBMs in a usual rider posture with a pre-impact braking event could potentially represent an additional large portion of crashes where an emergency avoidance maneuver occurs, underscoring the importance of understanding average rider postures and their variations in crash simulations.

Limitations

While this study provides valuable insights into the posture variations among PTW riders, the study has limitations affecting interpretation and applicability that requires acknowledgement. Due to constraints in time and resources, the sample size, both in terms of PTWs and volunteers, is one limitation, affecting the study's representativeness for the entire riding population. Postures were measured for three PTWs, where each PTW represent one model of a certain PTW type. This small sample size prevents the analysis from being extended to investigate posture variability within models of the same PTW type. Moreover, PTW types requiring postural adjustments at the spectrum's edges, like cruiser (feet forward) or super sport (excessive forward lean), were not considered.

The experimental setup, utilizing stationary PTWs within a controlled lab environment, introduces additional limitations. The volunteers were instructed to look straight ahead, because of this, the observed changes in head position does not account for the possible head movement necessary to scan surrounding traffic conditions, nor the possible influence from different helmet designs. Furthermore, dynamic factors previously shown to influence rider posture, such as balance, braking, and vibrations, were not accounted for (Ioannis et al. 2010; Tathe and Wani 2013).

The reliability and precision of the photometric skin marker-based method employed in this study is dependent on accurate marker placement. To avoid exposing volunteers to radiographic imaging, skeletal anatomical landmarks were located using the less accurate but harmless method of palpation. To minimize potential errors from markers sliding with the skin relative to the bone, marker placement and palpation were executed once volunteers were positioned on each PTW. However, this approach increases the variability introduced by palpation errors as the procedure is repeated for each PTW. Furthermore, the palpation procedure for each volunteer was

carried out by one of the two experienced physiotherapists, potentially introducing additional variability arising from the distinct identification of landmarks between the two professionals. However, their expertise enhances confidence in the accuracy and agreement of landmark identification.

In addition, examining the marker repetitions showed volunteers making slight posture adjustments between measurements. The longer time required for manually capturing hidden markers, collected separately, might contribute to increased variability. This is attributed to the extended time-frame, allowing volunteers additional opportunities to alter their postures, potentially impacting measurement consistency.

Acknowledgements

The authors would like to thank Instituto de Biomecánica (IBV) for conducting the measurements. The Instituto de Biomecánica (IBV) is a R+D+i center where the behavior of the human body is studied and its relationship with the products, environments and services that people use. The authors would also like to acknowledge BMW Motorrad, and Piaggio for supplying press photos of the touring and scooter PTWs.

Disclosure statement

No potential conflict of interest was reported by the author(s).

Funding

This work was financed by FFI (Strategic Vehicle Research and Innovation) under award number 2020-05153, by VINNOVA, the Swedish Transport Administration, the Swedish Energy Agency, and the Swedish vehicle industry.

ORCID

Linus Lundin  <http://orcid.org/0009-0008-5473-8306>
 Bengt Pipkorn  <http://orcid.org/0000-0002-9240-4517>
 Mats Y. Svensson  <http://orcid.org/0000-0002-8304-1398>
 Johan Iraeus  <http://orcid.org/0000-0001-9360-0707>

Data availability statement

The data that support the findings of this study are available in the form of the loadings and standard deviations of the scores of the first seven PCs.

References

- Ariffin AH, Solah MS, Hamzah A, Md Isa MH, Mohd Jawi Z, Md Yusoff NI, Hainin MR. 2016. Exploratory Study on Airbag Suitability for Low Engine Capacity Motorcycles. *J Teknol.* 78(4):65–69. doi:10.11113/jt.v78.7999.
- Arunachalam M, Mondal C, Singh G, Karmakar S. 2019. Motorcycle riding posture: a review. *Measurement.* 134:390–399. doi:10.1016/j.measurement.2018.10.019.
- Arunachalam M, Singh AK, Karmakar S. 2021. Perceived comfortable posture and optimum riding position of Indian male motorcyclists for short-duration riding of standard motorcycles. *Int J Ind Ergon.* 83:103135. doi:10.1016/j.ergon.2021.103135.

- Association of European Motorcycle Manufacturers [ACEM]. 2009. MAIDS: in-depth investigations of accidents involving powered two wheelers. Final report 2.0. Brussels (Belgium): ACEM. Available at: <http://www.maids-study.eu>.
- Barbani D, Baldanzini N, Pierini M. 2014. Development and validation of an FE model for motorcycle-car crash test simulations. *Int J Crashworthiness*. 19(3):244–263. doi:10.1080/13588265.2013.874672.
- Barberi E, Chillemi M, Cucinotta F, Sfravara F. 2023. Fast three-dimensional posture reconstruction of motorcyclists using openpose and a custom MATLAB script. *Sensors (Basel)*. 23(17):7415. doi:10.3390/s23177415.
- Barone S, Curcio A. 2004. A computer-aided design-based system for posture analyses of motorcycles. *J Eng Des*. 15(6):581–595. doi:10.1080/09544820410001731146.
- Bonkowski T, Hyncik L, Lv W. 2020. PTW passive safety: numerical study of standard impact scenarios with rider injury risk assessment. SAE Technical Paper (Paper no. 2020-01-0930). doi:10.4271/2020-01-0930.
- Bryant JT, Reid JG, Smith BL, Stevenson JM. 1989. Method for determining vertebral body positions in the sagittal plane using skin markers. *Spine (Phila Pa 1976)*. 14(3):258–265. doi:10.1097/00007632-198903000-00004.
- Capitani R, Pellari S, Lavezzi R. 2010. Design and numerical evaluation on an airbag-jacket for motorcyclists. *Int Conf. on ESAR, Hannover, Germany*. <https://opus4.hbz-nrw.de/opus45-bast/frontdoor/index/index/docId/510>.
- Chou J-R, Hsiao S-W. 2005. An anthropometric measurement for developing an electric scooter. *Int J Ind Ergon*. 35(11):1047–1063. doi:10.1016/j.ergon.2005.06.001.
- Claflin RA. 2002. Motorcycle rider posture prediction: the prediction of spinal curvature as a function of anthropometrics and point-of-contact chassis design [dissertation]. Orlando (FL): University of Central Florida. <https://search.proquest.com/openview/188c0857768205ecbabcbd0f02434ed9/1?pq-origsite=gscholar&cbl=18750&diss=y>.
- Federolf P, Reid R, Gilgien M, Haugen P, Smith G. 2014. The application of principal component analysis to quantify technique in sports. *Scand J Med Sci Sports*. 24(3):491–499. doi:10.1111/j.1600-0838.2012.01455.x.
- Gidion F, Carroll J, Lubbe N. 2021. Motorcyclist injuries: analysis of German in-depth crash data to identify priorities for injury assessment and prevention. *Accid Anal Prev*. 163:106463. doi:10.1016/j.aap.2021.106463.
- Han Y, Li Q, He W, Wan F, Wang B, Mizuno K. 2017. Analysis of vulnerable road user kinematics before/during/after vehicle collisions based on video records. IRCOBI Conference, Antwerp, Belgium. <https://www.ircobi.org/wordpress/downloads/irc17/pdf-files/26.pdf>.
- Huu DN, Ngoc VN. 2021. Analysis study of current transportation status in Vietnam's urban traffic and the transition to electric two-wheelers mobility. *Sustainability*. 13(10):5577. doi:10.3390/su13105577.
- International Organization for Standardization [ISO 13232-6:2005]. 2005. Motorcycles—test and analysis procedures for research evaluation of rider crash protective devices fitted to motorcycles—part 6: full-scale impact-test procedures.
- International Transport Forum [ITF]. 2015. Improving safety for motorcycle, scooter and moped riders. Paris (France): OECD Publishing Report No. <https://www.oecd-ilibrary.org/content/publication/9789282107942-en>.
- International Transport Forum [ITF]. 2022. Road safety annual report 2022. Paris (France): OECD Publishing Report No. <https://www.itf-oecd.org/sites/default/files/docs/irtad-road-safety-annual-report-2022.pdf>.
- Ioannis S, Gueven K, Filipe F, Van Rooij L, Erich S, Steffen P. 2010. Characterisation of motorcyclist's upper body motion during braking manoeuvre. IRCOBI Conference, Hannover, Germany. <http://www.ircobi.org/wordpress/downloads/irc0111/2010/Session4/4-9.pdf>.
- Izumiyama T, Nishida N, Yamagata H, Asahi R, Chen X, Ohgi J, Sugimoto S, Fukushima M. 2022. Analysis of individual variabilities for lumbar and pelvic alignment in highly reclined seating postures and occupant kinematics in a collision. IRCOBI Conference, Porto, Portugal. <http://www.ircobi.org/wordpress/downloads/irc22/pdf-files/22113.pdf>.
- Jolliffe IT, Cadima J. 2016. Principal component analysis: a review and recent developments. *Philos Trans A Math Phys Eng Sci*. 374(2065): 20150202. doi:10.1098/rsta.2015.0202.
- Kinescan/IBV. 2014. Ver. V2014. [software]. Valencia (Spain): IBV
- Langwieder K. 1977. Collision characteristics and injuries to motorcyclists and moped drivers. Stapp Car Crash Conference, New Orleans, Louisiana, USA. <https://www.sae.org/gsdownload/?prodCd=770920>.
- Maier S, Fehr J. 2024. Efficient simulation strategy to design a safer motorcycle. *Multibody Syst Dyn*. 60:289–316. doi:10.1007/s11044-023-09879-8.
- Maier S, Doléac L, Hertneck H, Stahlschmidt S, Fehr J. 2021. Finite element simulations of motorcyclist interaction with a novel passive safety concept for motorcycles. IRCOBI Conference, Online. <http://www.ircobi.org/wordpress/downloads/irc21/pdf-files/2117.pdf>.
- Maier S, Kemper F, Kronwitter S, Fehr J. 2022. Positioning and simulation of human body models on a motorcycle with a novel restraint system. IRCOBI Conference, Porto, Portugal. <http://www.ircobi.org/wordpress/downloads/irc22/pdf-files/2222.pdf>.
- MATLAB Statistics and Machine Learning Toolbox. 2023. Ver. R2023b. [software]. Natick (MA): the MathWorks Inc
- National Center for Statistics and Analysis [NCSA]. 2023. Motorcycles: 2021 data (traffic safety facts). Washington (DC): National Highway Traffic Safety Administration Report No: DOT HS 813 466. <https://crashstats.nhtsa.dot.gov/Api/Public/ViewPublication/813466>.
- Prochowski L, Pusty T. 2013. Analysis of motorcyclist's body movement during a motorcycle impact against a motor car side. *J Kones*. 20(4):371–379. doi:10.5604/12314005.1137849.
- Rab G, Petuskey K, Bagley A. 2002. A method for determination of upper extremity kinematics. *Gait Posture*. 15(2):113–119. doi:10.1016/S0966-6362(01)00155-2.
- Reed MP, Raschke U, Tirumali R, Parkinson MB. 2014. Developing and implementing parametric human body shape models in ergonomics software. Proceedings of the 3rd International Digital Human Modeling Conference, Tokyo, Japan. https://mreed.umtri.umich.edu/mreed/pubs/Reed_2014_DHM_Jack.pdf.
- Reed MP, Manary MA, Schneider LW. 1999. Methods for measuring and representing automobile occupant posture. SAE Technical Paper: 1999-1901-0959. doi:10.4271/1999-01-0959.
- Rogers NM, Zellner JW. 2001. Factors and status of motorcycle airbag feasibility research. ESV Conference, Amsterdam, Netherlands. <https://saemobilus.sae.org/content/2001-06-0102>.
- Sabbah AO, Bubb H. 2008. Development of a motorcycle posture model for DHM systems. Digital human modeling for design and engineering symposium, Pittsburgh (PA). doi:10.4271/2008-01-1866.
- Schaper D, Grandel J. 1985. Motorcycle collisions with passenger cars—analysis of impact mechanism, kinematics, and effectiveness of full face safety helmets. *SAE Trans*. 94:544–551. <http://www.jstor.org/stable/44467694>.
- Schneider LW, Robbins DH, Pflüg MA, Snyder RG. 1983. Development of anthropometrically based design specifications for an advanced adult anthropomorphic dummy family. Final Report. University of Michigan Transportation Research Institute, Ann Arbor, MI.
- Smith T, Zellner J, Rogers NM. 2006. A three dimensional analysis of riding posture on three different styles of motorcycle. International Motorcycle Safety Conference, Long Beach (CA). <https://msf-usa.org/wp-content/uploads/2023/03/a-three-dimensional-analysis-of-riding-posture-on-three-different-styles-of-motorcycle.pdf>.
- Snyder RG, Chaffin DB, Schutz RK. 1972. Link system of the human torso. Report No: HSRI-71-112/AMRL-TR-71-88. University of Michigan. <https://apps.dtic.mil/sti/tr/pdf/AD0754924.pdf>.
- Sporner A, Langwieder K, Polauke J. 1990. Passive safety for motorcyclists—from the legprotector to the Airbag. *SAE Int J Passeng Cars*. 99(Section 6):1064–1073. <https://www.jstor.org/stable/44554049>.
- Tathe SR, Wani KP. 2013. Modeling, simulation & analysis of whole body vibration for two wheeler. SAE Technical Paper: 2013-2001-2859. doi:10.4271/2013-01-2859.
- Thollon L, Godio Y, Bidal S, Brunet C. 2010. Evaluation of a new security system to reduce thoracic injuries in case of motorcycle accidents. *Int J Crashworthiness*. 15(2):191–199. doi:10.1080/13588260903102062.
- Van Auken RM, Kebschull SA, Broen PC, Zellner JW, Rogers NM. 2005. Development of a rider size and position model to determine motorcycle protective device test conditions. ESV Conference,

- Washington (DC). <https://citeseerx.ist.psu.edu/document?repid=rep1&type=pdf&doi=2cead73a719a4fa2b15c7c331dc09950d35ddd34>.
- Weinhandl JT, O'Connor KM. 2010. Assessment of a greater trochanter-based method of locating the hip joint center. *J Biomech.* 43(13):2633–2636. doi:10.1016/j.jbiomech.2010.05.023.
- Wisch M, Breunig S, Piantini S, Schick S, Whyte T, Brown J, Canu A, Perrin C, Serre T, Perera N. 2019. Protective Innovations of New Equipment for Enhanced Rider Safety (PIONEERS). Deliverable D1.1 Powered Two-Wheelers–Road Traffic Accident Scenarios and Common Injuries. Report No: 1.1. <https://pioneers-project.eu/wp-content/uploads/2020/12/Deliverable-D1.1.pdf>.
- World Health Organization Regional Office for South-East Asia [WHO]. 2015. Child development and motorcycle safety. W. H. Organization. Report No: 929022486X. <https://apps.who.int/iris/handle/10665/160762>.
- Zou H, Hastie T, Tibshirani R. 2006. Sparse principal component analysis. *J Comput Graph Stat.* 15(2):265–286. doi:10.1198/106186006X113430.